

The tilt of the local velocity ellipsoid as seen by *Gaia*

A. Everall,^{1★} N. W. Evans,^{1★} V. Belokurov¹ and R. Schönrich²

¹*Institute of Astronomy, University of Cambridge, Madingley Road, Cambridge CB3 0HA, UK*

²*University of Oxford, Rudolf Peierls Centre for Theoretical Physics, Clarendon Laboratories, Oxford OX1 3PU, UK*

Accepted 2019 August 5. Received 2019 July 11; in original form 2019 April 18

ABSTRACT

The *Gaia* Radial Velocity Spectrometer (RVS) provides a sample of 7224 631 stars with full six-dimensional phase space information. Bayesian distances of these stars are available from the catalogue of Schönrich, McMillan & Eyer. We exploit this to map out the behaviour of the velocity ellipsoid within 5 kpc of the Sun. We find that the tilt of the disc-dominated RVS sample is accurately described by the relation $\alpha = (0.952 \pm 0.007) \arctan(|z|/R)$, where (R, z) are cylindrical polar coordinates. This corresponds to velocity ellipsoids close to spherical alignment (for which the normalizing constant would be unity) and pointing towards the Galactic Centre. Flattening of the tilt of the velocity ellipsoids is enhanced close to the plane and Galactic Centre, whilst at high elevations far from the Galactic Centre the population is consistent with exact spherical alignment. Using the LAMOST catalogue cross-matched with *Gaia* DR2, we construct thin disc and halo samples of reasonable purity based on metallicity. We find that the tilt of thin disc stars straddles $\alpha = (0.909\text{--}1.038) \arctan(|z|/R)$, and of halo stars straddles $\alpha = (0.927\text{--}1.063) \arctan(|z|/R)$. We caution against the use of reciprocal parallax for distances in studies of the tilt, as this can lead to serious artefacts.

Key words: Galaxy: kinematics and dynamics – Galaxy: stellar content.

1 INTRODUCTION

Understanding the distribution of mass in the Milky Way is of great interest for constraining our Galaxy’s formation history. Unfortunately, the majority of the mass does not emit detectable electromagnetic radiation and so we are forced to use indirect methods. One such method is to analyse the velocity dispersion of stars, as this is related to the Galactic potential through the Jeans equations.

The sample of 7224 631 stars seen by the *Gaia* Radial Velocity Spectrometer (RVS; Brown et al. 2018; Katz et al. 2019) provides a tempting data set to study the behaviour of the velocity dispersion tensor. A recent attempt to do so was conducted by Hagen et al. (2019, henceforth H19). By augmenting the data set with multiple spectroscopic surveys, including LAMOST Data Release 4 (DR4; Cui et al. 2012), APOGEE DR14 (Abolfathi et al. 2018), and RAVE DR5 (Kunder et al. 2017), H19 generated a sample of the Solar neighbourhood in excess of 8 million stars. They found that the velocity ellipsoids of their sample were close to spherically aligned within the Solar radius, but became cylindrically aligned at larger radii.

The results of H19 show comparable total misalignment to Binney et al. (2014) using RAVE DR5 (Kunder et al. 2017). Both studies find that the tilt of the ellipsoids of their thin disc-dominated

samples deviate significantly from spherical alignment in the Solar neighbourhood. The mismatch is significantly greater than found by Büdenbender, van de Ven & Watkins (2015) using SEGUE G dwarfs (Yanny et al. 2009). The disagreement is more striking when compared to the halo population. A number of studies using Sloan Digital Sky Survey (SDSS) data (Adelmam-McCarthy et al. 2008) found an almost spherically aligned velocity ellipsoid for halo stars (Smith, Evans & An 2009; Bond et al. 2010; Evans et al. 2016). This seems to be confirmed by the recent study of Wegg, Gerhard & Bieth (2019), who used a set of RR Lyrae extracted from *Gaia* Data Release 2 (DR2) to conclude that the potential of the halo is spherical. This necessarily implies that the velocity ellipsoid is spherically aligned (Smith et al. 2009; An & Evans 2016). This is contrary to the results from H19, where the ellipsoid is cylindrically aligned at large distances from the Galactic Centre and high above the plane.

Here, we analyse the behaviour of the local velocity ellipsoid using the *Gaia* RVS, complemented with LAMOST. We introduce the data sets in Section 2, paying careful attention to distance errors and biases. We provide our algorithm in Section 3 and present our results in Sections 4 and 5. We find that simple use of the reciprocal of parallax as a distance estimator is dangerous and can lead to misleading results. The local velocity ellipsoid is always close to spherical alignment, and this remains true even for the thin disc and halo populations separately. The only substantial misalignment occurs for star samples at low latitudes and close to the Galactic Centre, where the potential is strongly disc dominated.

* E-mail: asfe2@cam.ac.uk (AE); nwe@ast.cam.ac.uk (NWE)

2 DATA

2.1 The *Gaia* DR2 RVS sample

The *Gaia* DR2 RVS sample is a subset of the main DR2 catalogue with radial velocities derived from the on-board spectrograph (Brown et al. 2018; Katz et al. 2019). Although this gives us six-dimensional phase space data for over 7 million stars, the information on the distance is of course encoded as the parallax [an introductory discussion how to infer distances from *Gaia* parallaxes can be found in Luri et al. (2018) and Bailer-Jones (2015)]. To recover the tilt of the velocity ellipsoid, special care needs to be taken with the inferred distances. Of course, to convert the proper motions into the tangential velocities requires the distance, and so poorly computed and noisy distances can overwhelm calculations of the tilt. We thus face two central problems: (i) the parallaxes of *Gaia* can be biased and (ii) the method of inferring distances can be biased.

Concerning the parallax bias, Lindegren et al. (2018) used a sample of known quasars to determine a zero-point parallax offset of $\delta_{\varpi} = -29 \mu\text{as}$, whilst they also showed that the parallax uncertainties are underestimated by about $\delta\sigma_{\varpi} = 43 \mu\text{as}$, which are to be added in quadrature. The offset is known to depend on colour and apparent magnitude, might also depend on the object type and parallax, and hence is likely inappropriate for stellar objects in the RVS catalogue. More appropriate to the RVS catalogue, but still restricted to a particular subsets of stars, are a series of papers that found different parallax offsets: Riess et al. (2018) constrained $\delta_{\varpi} = -46 \pm 13 \mu\text{as}$ for Cepheids, whilst Xu et al. (2019) found a value of $-75 \pm 29 \mu\text{as}$ using VLBI astrometry of Young Stellar Objects (YSOs) and pulsars. Zinn et al. (2019) and Khan et al. (2019) use asteroseismology for (mostly) red giants in the Kepler fields to get parallax offsets $\sim -50 \mu\text{as}$, depending on the field position. For the full *Gaia* DR2 RVS sample, the parallax offset was calculated by Schönrich, McMillan & Eyer (2019, henceforth S19) using their statistical distance method. They find an average parallax offset of $-54 \pm 6 \mu\text{as}$, where the uncertainty comprises their systematic uncertainty with a negligible statistical error.

The literature contains in principle four approaches to infer stellar distances:

(i) Simply setting the distance $s = 1/\varpi$, as done by H19. This approach should only be used in situations where the parallax uncertainty is negligible for the problem, since it produces a threefold bias: neglect of the selection function, neglect of the spatial distribution of stars, and ignorance of the fact that $1/\varpi$ is not the expectation value of the probability distribution function $P(s)$. The latter bias was already identified by Strömberg (1927) and became later well known as the Lutz & Kelker (1973) bias.

(ii) Performing Bayesian distance estimates with a set of generic assumptions about the sample and the underlying Galactic density distribution, which eliminates the major problems of $s = 1/\varpi$, but leaves some uncertainties concerning the selection function. A good example of this approach is Bailer-Jones et al. (2018).

(iii) Doing a full Bayesian estimate involving stellar models, such as the Anders et al. (2019) distances.

(iv) Doing a full Bayesian approach with a self-informed prior that estimates the selection function from the data directly (Schönrich & Aumer 2017; S19). Speaking generally, approaches (iii) and (iv) yield the most trustworthy results, though they of course involve greater expenditure of effort.

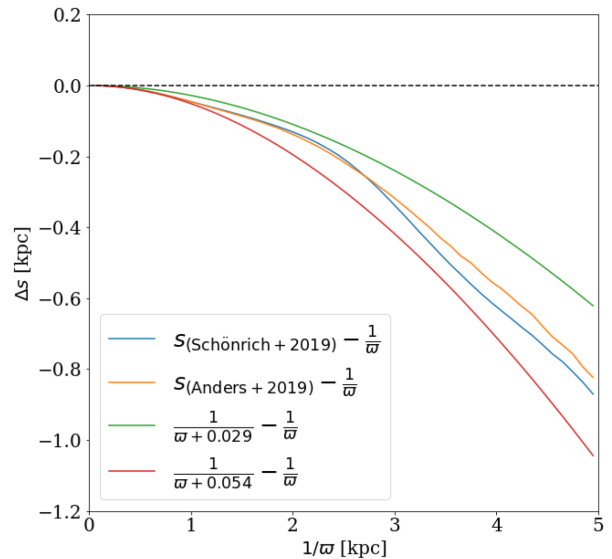


Figure 1. Running median of the distance offset from a naive parallax reciprocal. The green curve is generated by corrections using the $29 \mu\text{as}$ parallax offset suggested by Lindegren et al. (2018), whilst the red curve uses the $54 \mu\text{as}$ parallax offset suggested by S19. Finally, the blue and orange curves show the difference between the parallax reciprocal and the Bayesian distance estimates from S19 and A19, respectively. Using the reciprocal of the parallax as a distance estimator is unwise beyond heliocentric distances $s \sim 1 \text{ kpc}$.

The mean bias between the different δ_{ϖ} estimates, and distance estimators is shown in Fig. 1. The S19 distances deviate from a simple parallax reciprocal $1/\varpi$ for distances beyond $\sim 1 \text{ kpc}$. They also show substantially greater offset than would be accounted for by the $29 \mu\text{as}$ correction. We also note that the distance deviation is smaller than if we were to use the $54 \mu\text{as}$ offset and naively use $1/\varpi$. Fig. 1 underscores the point that the crude calculation of $1/\varpi$ overestimates the distance.

Tangential velocities are calculated by multiplying the proper motion by the distance whilst the spectroscopically determined radial velocities are independent of distance. If for example the true distance is underestimated (or overestimated), then so will be the tangential velocities. When inferring the velocity ellipsoid using spectroscopic radial velocities, this will tend to lead to heliocentrically aligned velocity ellipsoids, i.e. the velocity ellipsoids will become elongated (or compressed) towards the solar position. From Fig. 1, we see that using $s = 1/\varpi$ overestimates distances therefore will enhance the tangential velocities and cause the velocity ellipsoids to circularise around the Solar position. Notably, the result would be a flattening of the tilt of the velocity ellipsoids at the Solar radius as observed by H19.

We use the Bayesian distance estimates derived by S19 for our RVS sample. The data set includes corrected parallaxes and parallax uncertainties, which were also revised upwards by S19, and which we use to make quality cuts when applying to this data. Following common practice for parallax-based distance sets, we use $\varpi/\sigma_{\varpi} > 5$.¹ We select only stars within 5 kpc of the Sun ($\varpi > 200 \mu\text{as}$ or $s < 5 \text{ kpc}$ for the Bayesian distances). To remove spurious line-of-sight velocity outliers, we apply $\sigma_{v_r} < 20 \text{ km s}^{-1}$ as well as $|v_r| <$

¹S19 helpfully provide a ϖ/σ_{ϖ} parameter with revised σ_{ϖ} , which we use to cut on parallax signal-to-noise ratio when applying their distance estimates.

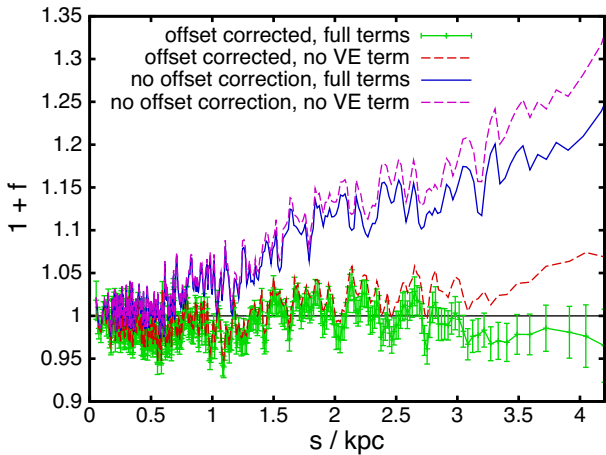


Figure 2. A scan of the *Gaia* RVS for the fractional distance error $1 + f$ versus distance s with the quality cuts described in S19. Just as in S19, we move a mask of 12 000 stars in steps of 4000 stars over the sample. The green error bars show the distance statistics after the distance correction, whilst the solid line shows the statistics when no parallax offset correction is applied. For both values of δ_{ϖ} , we show with dashed lines the same statistics when we completely remove the velocity ellipsoid correction term, which is equivalent to the wrong assumption that the velocity ellipsoid is cylindrically aligned. The resulting difference overestimates the actual uncertainty, but is still comparably small.

500 km s^{-1} and further follow the recommendations of Boubert et al. (2019), which remove stars with less than 4 RVS transits and bright neighbours that can contaminate the measurements.

A concern with S19 distance estimates is that the kinematic model prior used to calculate the distances assumed a radially aligned velocity ellipsoid. If this assumption was dominant in the distance inference, our results would be heavily biased towards finding a spherically aligned velocity ellipsoid. We address this concern in two ways. First, we compare S19 distance estimates with those found by Anders et al. (2019, henceforth A19) from photoastrometric distances using the StarHorse pipeline (Queiroz et al. 2018). The potential biases between the S19 and A19 distances are very different. The latter set profits in precision from stellar model priors, whilst it may also inherit biases from the stellar models and have less well-defined distance uncertainties. These two data sets provide an excellent mutual control for remaining biases on either side. To correct for the parallax offset, A19 linearly interpolate as a function of G -band magnitude between the Lindegren et al. (2018) value of $29 \mu\text{as}$ at $G = 16.5$ and the $50 \mu\text{as}$ offset found by Zinn et al. (2019) at $G = 14$. We place the same cuts to the data set using A19 distances as described earlier, but using a signal-to-noise cut-off $s/\sigma_s > 5$ on heliocentric distance rather than parallax. The A19 distance estimates are also in Fig. 1. The estimates are similar to S19 within 3 kpc, where the inference in both methods is dominated by parallax information with low uncertainties. Outside 3 kpc, the distance estimates of A19 are systematically larger by ~ 0.1 kpc. It is unclear where this disagreement originates from however we find it to be a small enough shift that our results are not significantly affected. In Section 4, we calculate the tilt for RVS data from StarHorse distances and find it to be consistent with that measured with S19.

Secondly, to truly quench any remaining uncertainty and to reinforce the use of $54 \mu\text{as}$ offset, we test the effect of the velocity ellipsoid correction terms on distance bias found in S19. This is shown in Fig. 2, where we plot the measured average distance bias versus distance for the S19 distances calculated with and without the

parallax offset. The dashed lines show the ‘measured’ distance bias, when we completely remove the velocity ellipsoid correction (which is equivalent to the wrong assumption that the velocity ellipsoid has a perfect cylindrical alignment).

Two things are obvious: (i) Even with such a drastic error in assumptions, the change to the distance statistics is less than a third of the overall correction. As a result, the uncertainty in the velocity ellipsoid correction term is more than an order of magnitude smaller than the measured value of the parallax offset in S19. This is also reflected in the systematic uncertainty budget provided by S19. (ii) When neglecting the velocity ellipsoid correction term, we actually require a larger correction for the parallax offset. As subsequent analysis will show, larger parallax offsets tend to flatten ellipsoids towards the Galactic Centre and increase the tilt of ellipsoids around and outside the Solar radius. Hence, this only strengthens our conclusion that the flattening of the tilt at the solar radius reported by H19 is driven by biased distance estimates.

2.2 The LAMOST DR4 and *Gaia* DR2 cross-match

We separately analyse the velocity ellipsoids generated from the combination of five-dimensional phase space information from *Gaia* DR2 (Brown et al. 2018), together with radial velocities from the LAMOST DR4 value added catalogue (Cui et al. 2012; Xiang et al. 2017). This enables us to analyse the velocity ellipsoids with an independent catalogue of stars. LAMOST also provides metallicity estimates, which we use to produce halo and thin disc samples by cutting on $[\text{Fe}/\text{H}] < -1.5$ and $[\text{Fe}/\text{H}] > -0.4$, respectively, as done in H19.

We apply the same cuts to this data set as for RVS, namely $\varpi/\sigma_{\varpi} > 5$, $\varpi > 200 \mu\text{as}$, $\sigma_{v_r} < 20 \text{ km s}^{-1}$, and $v_r < 500 \text{ km s}^{-1}$. In the region of overlap between *Gaia* RVS and LAMOST, we use the radial velocity estimate with the least uncertainty.

We should be cautious of the radial velocities in LAMOST due to the statistical analysis performed by Schönrich & Aumer (2017). They determined that the LAMOST radial velocities were offset high by $\sim 5 \text{ km s}^{-1}$. Assuming this offset is global throughout the data set, it would shift our mean velocities without significantly impacting the velocity dispersions. Hence, we do not include this offset in our analysis.

3 METHOD

To transform from heliocentric to Galactocentric coordinates, we need to fix some Galactic constants. We assume a Solar position² in cylindrical polar coordinates of $(R_{\odot}, z_{\odot}) = (8.27, 0.014)$ kpc (e.g. Binney, Gerhard & Spergel 1997). The circular velocity of the Local Standard of Rest is taken as $v_c(R_{\odot}) = 238 \text{ km s}^{-1}$ (Schönrich 2012), whilst the Solar peculiar motion is $(U_{\odot}, V_{\odot}, W_{\odot}) = (11.1, 12.24, 7.25) \text{ km s}^{-1}$ (Schönrich, Binney & Dehnen 2010).

We determine the velocity ellipsoid parameters using maximum likelihood estimation on the bivariate Gaussian likelihood function convolved with Gaussian measurement uncertainties similar to previous works (e.g. Bond et al. 2010; Evans et al. 2016; H19). We resolve the velocities into Galactocentric spherical polar coordinates

²The effect of changing the Solar position is investigated in Section 5.1.

(v_r, v_θ, v_ϕ) and use a likelihood function:

$$\log \mathcal{L} = -\frac{1}{2} \log |2\pi\Lambda| - \frac{1}{2} \sum_i (\mathbf{x}_i - \boldsymbol{\mu})^T \Lambda^{-1} (\mathbf{x}_i - \boldsymbol{\mu}). \quad (1)$$

Here, $\mathbf{x}_i = (v_{r,i}, v_{\theta,i})$ are the velocity components of the i th star, and $\Lambda = \Sigma + \mathbf{C}$, where Σ is the velocity covariance matrix in (v_r, v_θ) and \mathbf{C} the measurement uncertainty covariance matrix of the data. The data are binned in a 20×20 grid of Galactocentric cylindrical polar coordinates (R, z) , such that each bin is approximately 500×500 pc. For every bin, we analytically calculate the means and covariances of the contained populations without measurement uncertainties. These parameters are used to initialize our likelihood optimization in order to calculate a best-fitting model with the uncertainties. The algorithm proceeds by optimizing the means and covariances for each bin independently.

For the measurement errors in the RVS sample, we take the standard deviation and correlation parameters for parallaxes, radial velocities, and proper motions from the *Gaia* DR2 data set. The challenge here is that our likelihood function is inherently Gaussian, whilst, assuming parallax uncertainties are Gaussian, the distance uncertainty distribution is inherently non-Gaussian. When using $1/\varpi$ as our distance estimator, the parallax uncertainty is propagated so we do not assume Gaussian distance uncertainties. However, we do assume Gaussian velocity uncertainties when calculating the likelihood function. When using distance estimates from S19, it is important to use the correct uncertainty distribution. For the purposes of this work, we assume Gaussian distance uncertainties using the second moment of distance given by S19 as the variance. For future work, it will be important to understand the impact of the third and fourth moments of distance on our velocity ellipsoids. We also assume here that the distance is uncorrelated with the remaining astrometric parameters. For the LAMOST cross-matched with *Gaia* sample, we assume that radial velocities are uncorrelated with all the *Gaia* astrometric parameters.

We determine the parameter posteriors by using the MCMC PYTHON package `emcee` (Foreman-Mackey et al. 2013). We find that initializing walkers in a small ball around our analytically determined parameters allows the chains to converge within 50 iterations. We run 20 walkers for 300 iterations and use the last 150 to calculate our posteriors.

4 RESULTS

4.1 The *Gaia* DR2 RVS sample

For our analysis of the *Gaia* RVS sample, we compute the velocity ellipsoids for three different assumptions to show the effects of distance errors:

- (i) Without any parallax correction and using $s = 1/\varpi$,
- (ii) With a parallax correction of $29 \mu\text{as}$ and using $s = 1/\varpi$,
- (iii) With the Bayesian distance estimates from S19, which use a parallax correction of $54 \mu\text{as}$.

Our total sample sizes after applying cuts are 5375 902, 5499 054, and 5221 912, respectively. The velocity ellipsoids produced using assumptions (i) and (ii) are shown in Fig. 3, whilst those produced using (iii) are given greater prominence in Fig. 4. We only show ellipsoids in bins with greater than 30 stars, as these still provide clean results and allow us to view the distribution out to greater distances.

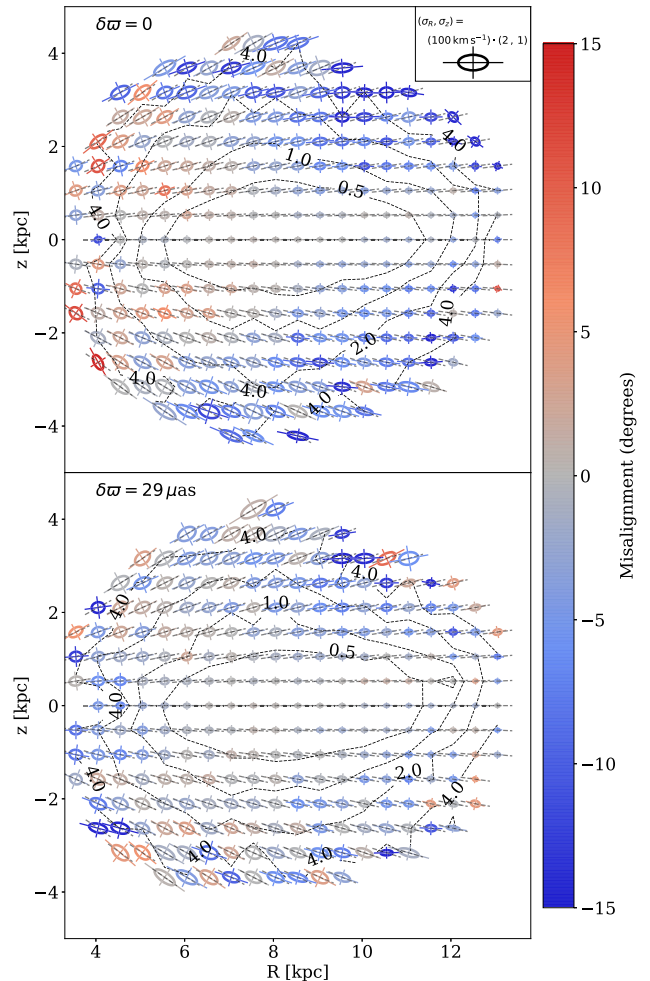


Figure 3. Velocity ellipsoids generated from the *Gaia* RVS DR2 data set with different treatments of parallax bias. The size of the ellipsoid is proportional to the value of the velocity dispersion in each bin. The short-dashed lines correspond to the orientation of a spherically aligned velocity dispersion, whilst the colour bar gives the deviation in degrees of the velocity ellipsoid orientation from this spherical alignment, with blue indicating a flattening and red an over-tilting towards the disc. The black dashed lines show contours of misalignment uncertainty. Top: Using distance as $1/\varpi$ with no parallax offset correction. Bottom: Distance as $1/\varpi$ with $29 \mu\text{as}$ parallax correction.

In the top panel of Fig. 3, we recover fig. 2 of H19. We see the same transition from approximate spherical to cylindrical alignment across the Solar radius. We note that our results are somewhat more noisy, since we have not augmented our data set with spectroscopic catalogues and so our sample is about 75 per cent of the size of H19. This effect is consistent with overestimates of the distances, and hence tangential velocities, as already discussed in Section 2.1. The bottom panel of Fig. 3 shows the same results with a $29 \mu\text{as}$ correction. The behaviour of the velocity ellipsoid is now much more consistent throughout the meridional plane, without the awkward transition from spherical to cylindrical alignment at the Solar circle. However, of course this correction is conservative and not physically motivated for stars in the RVS sample.

Fig. 4 uses the Bayesian distance estimates from S19 and is the centrepiece of our results. We note that the ellipsoids do not extend out as far as in the previous plots. The reason for this

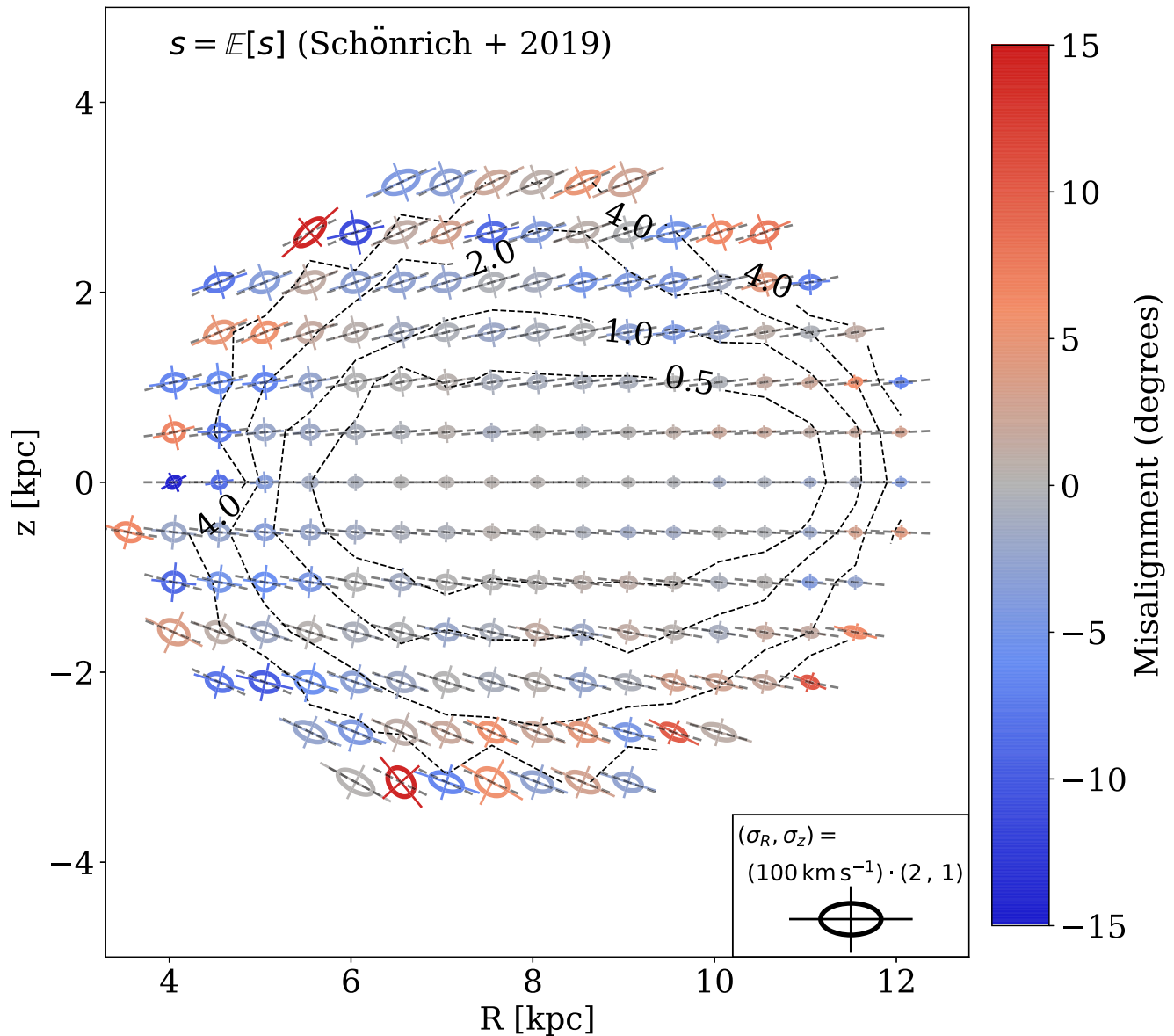


Figure 4. Velocity ellipsoids generated from the *Gaia* RVS DR2 with Bayesian distance estimates from S19, which include a parallax offset correction of $54 \mu\text{s}$. This figure can be compared to Fig. 3 that make inferior assumptions as to the distance estimates. Black dashed contours give the ellipsoid orientation uncertainty for 0.5° , 1° , 2° , and 4° , respectively. Note that the artificial transition from spherical to cylindrical alignment at the Solar circle visible in the upper panel of Fig. 3 has been removed.

is that S19 also revise the parallax uncertainty upwards. As a consequence, when cutting on parallax uncertainty $\varpi/\sigma_\varpi > 5$, we remove more stars, particularly at large distances. Those bins which are no longer included do not contain a requisite number of stars for us to plot the ellipsoids. We do observe a slight deviation of the spherical alignment of the velocity ellipsoids at low elevation towards inner radii, tending to cylindrical alignment. This is likely the effect of the contribution of the baryonic disc to the gravitational potential. The same effect can be seen in the velocity ellipsoids of RR Lyrae in the halo in Wegg et al. (2019), although most of the effect in their analysis occurs within 4 kpc of the Galactic Centre, outside of which the velocity ellipsoids appear to be spherically aligned.

Notice that the size of the velocity ellipsoids increases with elevation above and below the plane. This is caused by the inclusion of three populations of stars, belonging to the thin disc, thick disc, and halo. It is interesting to look at the populations separately, and for this we turn to the LAMOST and *Gaia* cross-matched sample, which has spectroscopic metallicities.

4.2 The LAMOST DR4 and *Gaia* DR2 cross-match

Without Bayesian distances for this sample, we use $s = 1/\varpi$ as our estimator with parallax corrections 29 and $54 \mu\text{s}$. We expect these to overestimate and underestimate distances, respectively, as indicated by Fig. 1. Therefore, our results on the tilt of the velocity ellipsoid merely bracket the range of possibilities.

We split the sample into two separate populations, $[\text{Fe}/\text{H}] > -0.4$ as a thin disc sample and $[\text{Fe}/\text{H}] < -1.5$ as a halo sample. Neither sample is completely pure, as the metallicity cuts only approximately separate populations. After applying the cuts, our halo samples contain 18 424 and 19 661 stars for $29\mu\text{s}$ and $54\mu\text{s}$ corrections respectively and the thin disc samples contain 2286 528 and 2306 729 stars.

In Fig. 5, we present results for the thin disc sample. In the left plot, the flattening of the tilt is still strong for the $29\mu\text{s}$ correction, with cylindrical alignment particularly prevalent at elevations above 2 kpc from the plane. In the right plot, with a $54\mu\text{s}$ correction, the majority of this signal has been removed. However, there appears to be a small but significant deviation from spherical alignment remaining for heights $|z| \sim 2.5$ kpc. It is suggestive that there the thin disc population may not be exactly spherically aligned.

The results for the low-metallicity halo sample are given in Fig. 6. This contains a much smaller number of stars, which allows us fewer bins and causes the results to appear more noisy. However, in the left plot, with the conservative $29\mu\text{s}$ correction, almost cylindrical alignment can be seen for $R \sim 10$ kpc and $z \sim 2$ kpc that is completely removed in the right-hand plot for the $54\mu\text{s}$ overcorrection. We also note here that the scales of the velocity dispersions are much more consistent across elevations that demonstrates the effect of selection of the halo sample with only small impurities.

5 THE TILT OF THE VELOCITY ELLIPSOID

Binney et al. (2014) and Büdenbender et al. (2015) introduced and exploited a compact way to summarize results on the tilt of the velocity ellipsoids. They used a model in which the angle between the Galactic plane and the direction of the longest axis of the velocity ellipsoid is

$$\alpha = \alpha_0 \arctan |z|/R. \quad (2)$$

They fitted the binned data to the model to determine the best fit α_0 parameter. A result of $\alpha_0 = 1$ implies exact spherical alignment, whilst $\alpha_0 < 1$ means that the ellipsoids are tilted towards cylindrical alignment.

We perform a least squares regression on all bins with $n_{\text{stars}} > 5$ as these still contain valuable information about ellipsoid alignment although with large uncertainties.³ Bins with fewer stars are almost randomly aligned. For the *Gaia* RVS sample with S19 distances, we acquire a tilt value of $\alpha_0 = 0.952 \pm 0.007$. This is in significant disagreement with $\alpha_0 \sim 0.8$ determined in Binney et al. (2014) from the local RAVE stars (Steinmetz et al. 2006). It is in reasonable agreement with Büdenbender et al. (2015), who found a value of 0.90 ± 0.04 using the Segue G dwarf sample. As discussed in Section 2, we also calculate this parameter for the distance estimates of A19 with the RVS sample and retrieve $\alpha_0 = 0.956 \pm 0.006$, in remarkably good agreement with the estimate from S19 distances.

We see no physical reason why this parameter should be constant across all populations of stars and in all parts of the Galaxy. Under the hypothesis that tilt of the velocity ellipsoids is controlled at least in part by the contribution of the baryonic disc to the potential, we anticipate that α_0 should be lowest near the plane and tend towards

³In Section 4, we only use bins with $n_{\text{stars}} > 30$ because the scatter in less populated bins make the ellipsoid plots appear untidy and muddled the trends in behaviour.

1 at high elevation. We also suggest that the flattening of the tilt should be more extreme in the inner radii. To test this hypothesis, we compute α_0 for subsets of our velocity ellipsoids. We find that for $|z| < 2$ kpc, $\alpha_0 = 0.950 \pm 0.007$, whilst for $|z| > 2$ kpc, $\alpha_0 = 0.966 \pm 0.018$. We also find that at $R < 7$ kpc, $\alpha_0 = 0.917 \pm 0.013$, whilst for $R > 7$ kpc, $\alpha_0 = 0.963 \pm 0.007$. This is consistent with the hypothesis that the effects of the disc potential are driving much of the deviation from spherical alignment.

We also look at the tilt at large radii and high elevation. For $|z| > 2$ kpc and $R > 7$ kpc, we retrieve the result $\alpha_0 = 0.986 \pm 0.020$, which is consistent with spherical alignment. This is in good agreement with a number of studies of the velocity ellipsoids of halo stars in SDSS (Smith et al. 2009; Bond et al. 2010; Evans et al. 2016), as well as the recent work of Wegg et al. (2019) who determined that the kinematics of the RR Lyrae in the halo, extracted from *Gaia* DR2, imply a spherically symmetric halo potential.

In Fig. 7, we show the fit of the tilt of the velocity ellipsoids as a function of $|z|/R$. The green solid line shows the expected trend for spherical alignment ($\alpha_0 = 1$). We plot our best fit, as well as the earlier results from Binney et al. (2014) and Büdenbender et al. (2015). The blue points are the posterior means of uncertainties of ellipsoid inclinations and misalignments in $|z|/R$ bins. Notice that the binned data points show an interesting pattern with respect to the best fit. The data points with high $|z|$ mostly lie just above the best fit, those with low $|z|$ lie just below. This trend suggests that the deviations from spherical alignment are induced by the disc potential.

We also compare ellipsoids above and below the plane. We find that above the disc $\alpha_0 = 0.964 \pm 0.009$, whilst below the plane, $\alpha_0 = 0.940 \pm 0.009$, showing 2σ disagreement. However, this asymmetry is far more stark when separating in-plane from high elevation contributions. Considering only ellipsoids within 1 kpc of the plane, we find that $\alpha_0 = 0.989 \pm 0.014$ above and 0.888 ± 0.013 below that has a 5σ difference. Conversely, outside 1 kpc, $\alpha_0 = 0.94 \pm 0.01$ and 0.99 ± 0.01 above and below, respectively, in 3σ disagreement and opposite to the in-plane difference.

For an axisymmetric equilibrium that is reflexion symmetric about the Galactic plane, results above and below the plane should be consistent. This apparent discrepancy particularly in the disc may be caused by substructure and streams, buckling of the Galactic bar (Saha, Pfenniger & Taam 2013), or by the effects of bending modes in the disc (e.g. Gómez et al. 2013; Williams et al. 2013; Xu et al. 2015; Laporte et al. 2019), or by unrecognized systematics in the data.

We analyse the thin disc and halo samples generated from the *Gaia*-LAMOST cross-match. For the disc sample, we recover $\alpha = 0.909 \pm 0.008$ for the $29\mu\text{s}$ correction, which becomes $\alpha = 1.038 \pm 0.008$ for the $54\mu\text{s}$ correction. As anticipated, this straddles the RVS results, demonstrating the effect of overestimating and underestimating the distances. The same effect is present in the halo sample with $\alpha = 0.927 \pm 0.035$ and $\alpha = 1.063 \pm 0.036$ for corrections of 29 and $54\mu\text{s}$, respectively.

5.1 The Solar position

In the analysis, we assumed a Solar distance to the Galactic Centre of $R_\odot = 8.27$ (Binney et al. 1997) and neglected uncertainties on this estimate. This is mainly to ease comparison with earlier work, especially H19. Recently, the Gravity Collaboration et al. (2018) reported a high-precision distance to Sagittarius A* of 8.127 ± 0.031 kpc, which is smaller than our assumed value.

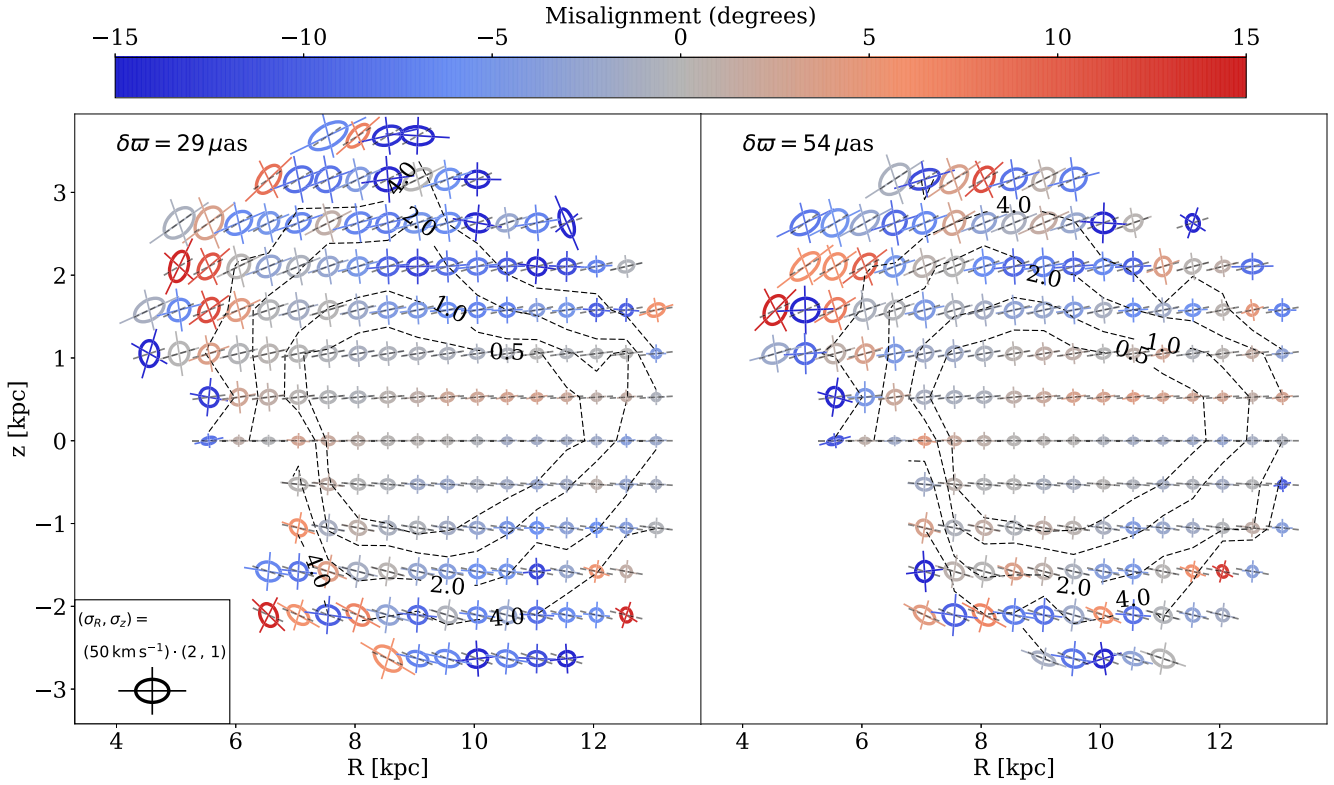


Figure 5. Velocity ellipsoids generated from *Gaia* DR2 cross-matched with LAMOST with $[\text{Fe}/\text{H}] > -0.4$, producing a thin disc sample. As usual, the size of the ellipse is related to the value of the velocity dispersion in the given spatial bin. The colour corresponds to the deviation in degrees of the velocity ellipsoid orientation from spherical alignment. In other words, grey implies spherical alignment whilst blue implies tending towards cylindrical alignment. The black dashed contour shows the misalignment uncertainty. We use $1/\omega$ as a distance estimator but with $29 \mu\text{as}$ correction (left-hand panel) and $54 \mu\text{as}$ correction (right-hand panel). These bracket the range of possibilities, as the former overestimates and the later underestimates the true distances.

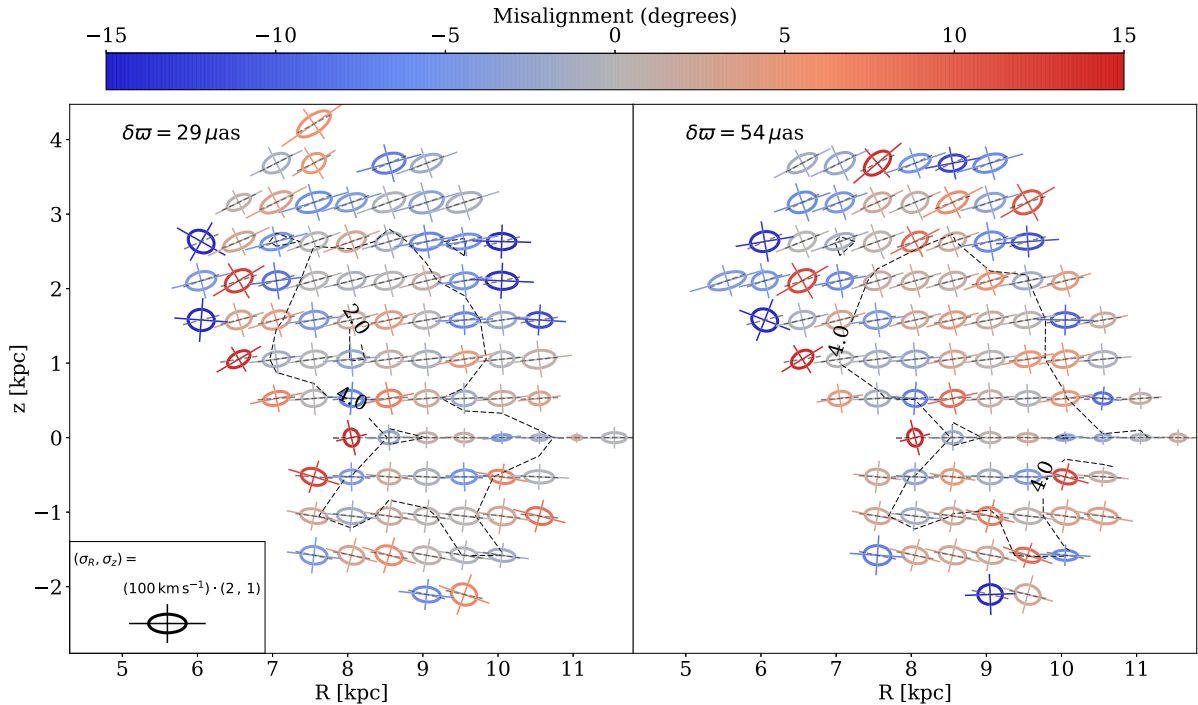


Figure 6. As Fig. 5, but for the halo sample obtained from *Gaia* DR2 cross-matched with LAMOST with $[\text{Fe}/\text{H}] < -1.5$.

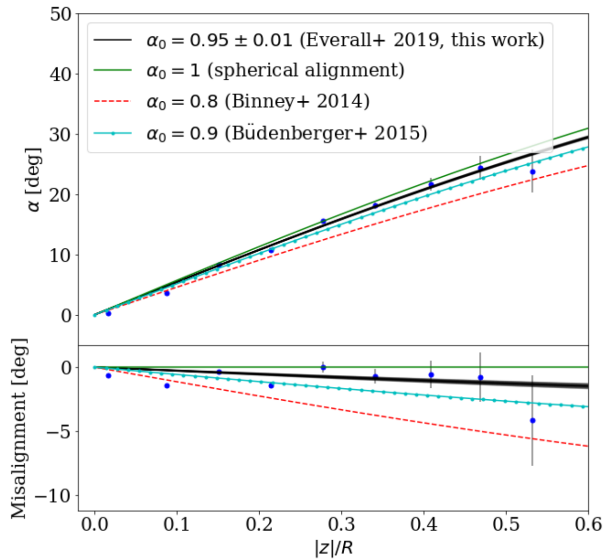


Figure 7. The upper panel shows fits for the tilt of the velocity ellipsoid using equation (2). The blue points provide the posterior means and uncertainties of ellipsoid inclinations in $|z|/R$ bins. Perfect spherical alignment corresponds to the green line, whereas the black line is our result from the *Gaia* RVS sample with distances from S19. For comparison, we also show recent fits from Binney et al. (2014) (red) and Büdenbender et al. (2015) (pale blue). Notice that the binned data points show a transition from below to above the best-fitting line, as the disc potential becomes less dominant. The lower panel shows the deviation from spherical alignment.

Adjusting the Solar position with respect to the Galactic Centre does not change the properties of velocity ellipsoids in Cartesian coordinates. The only impact is that we now calculate the misalignment with respect to a new central point in the Galaxy.

For this change in R_{\odot} , the shift in misalignment is small. In the most extreme cases of velocity ellipsoids at ($|z| \sim 2$, $R \sim 4$) kpc, the misalignment is reduced by 0.84° that falls well within our uncertainties. On average, across all our ellipsoid positions, the induced flattening is 0.33° . The effect on any individual ellipsoid is negligible.

However, a change in R_{\odot} induces a coherent shift in all ellipsoid misalignments, and so there is a somewhat larger effect on our inference of the tilt normalization parameter, α_0 . We find that using $R_{\odot} = 8.127$ kpc, the full RVS sample generates a tilt parameter of $\alpha_0 = 0.953 \pm 0.007$. This shift is still within the original uncertainties. Similar calculations for subsamples of the ellipsoids prove even less significant due to their increased uncertainties.

6 CONCLUSIONS

The tilt of the velocity ellipsoid of local stars is important for several reasons. First, determinations of the local dark-matter density are usually based on the vertical kinematics of stars. The gravitational potential is inferred from the Jeans equations or distribution functions, a calculation known to be sensitive to the tilt of the velocity ellipsoid (e.g. Silverwood et al. 2016; Sivertsson et al. 2018). Secondly, the heating processes that thicken discs include scattering by in-plane spiral arms and by giant molecular clouds. These scattering processes can produce different signatures in the tilt of the thin disc velocity ellipsoid (e.g. Sellwood 2014). Thirdly, the alignment can give direct information on the potential in some instances (e.g. Eddington 1915; Binney & McMillan 2011).

For example, the halo stars are believed to be close to spherical alignment, as judged by a number of earlier studies of SDSS star samples (e.g. Bond et al. 2010). Exact spherical alignment implies a spherically symmetric force field (Smith et al. 2009; An & Evans 2016).

The *Gaia* RVS sample comprises 7224 631 stars with full-phase space coordinates. The main hurdle to overcome in exploiting this data set to study the tilt is the accurate and unbiased conversion of parallaxes ϖ to heliocentric distances s . We find that the Bayesian distances of S19, which incorporate a parallax offset of $54 \mu\text{as}$, give reliable results. We have checked that substitution of photoastrometric distances from A19 using the StarHorse pipeline gives consistent results. However, use of the reciprocal of parallax as a distance estimator leads to artefacts in the behaviour of the inferred velocity ellipsoids and this practise should be deprecated.

The *Gaia* RVS sample is consistent with nearly spherical alignment. The tilt is accurately described by the relation $\alpha = (0.952 \pm 0.007) \arctan(|z|/R)$. If the normalizing constant were unity, then this would imply exact alignment with spherical polars. Our result is pleasingly close to that found by Büdenbender et al. (2015) from the Segue G dwarf stars in the Solar neighbourhood. If the sample is restricted to stars at large Galactocentric radii, or great distances above or below the plane, then the alignment becomes still closer to spherical. The data support the conjecture that any deviation from spherical alignment of the velocity ellipsoids is caused by the gravitational potential of the disc. Such deviations occur at low $|z|$ and close to the Galactic Centre, whilst at $|z| > 2$ kpc and $R > 7$ kpc the ellipsoids are consistent with spherical alignment.

Subsamples from *Gaia* DR2 cross-matched with LAMOST enable us to study the disc and halo populations separately. Even though Bayesian distances are not available for all these stars, we can bracket the tilt of the velocity ellipsoids by making assumptions that underestimate and overestimate the heliocentric distances. For thin disc stars, we find $\alpha = (0.909-1.038) \arctan(|z|/R)$ and for halo stars $\alpha = (0.927-1.063) \arctan(|z|/R)$. Both populations are close to spherical alignment, with the only real deviations occurring in the inner Galaxy near the Galactic plane.

Here, we have studied only the orientation of the velocity ellipsoids as seen by *Gaia*. Our results have important implications for the local dark-matter density, for which treatment of the tilt term is a major source of the uncertainty. We plan to attack this problem in a forthcoming publication.

ACKNOWLEDGEMENTS

AE thanks the Science and Technology Facilities Council of the United Kingdom for financial support. This work was partly performed at the Oxford *Gaia* sprint, and we thank Douglas Boubert and Payel Das for organising the meeting. The work was completed at the Kavli Institute for Theoretical Physics, Santa Barbara. NWE and VB acknowledge support in part by the National Science Foundation under grant no. NSF PHY-1748958.

REFERENCES

- Abolfathi B. et al., 2018, *ApJS*, 235, 42
- Adelmam-McCarthy J. K. et al., 2008, *ApJS*, 175, 297
- An J., Evans N. W., 2016, *ApJ*, 816, 35
- Anders F. et al., 2019, preprint (arXiv:1904.11302) (A19)
- Bailer-Jones C. A. L., 2015, *PASP*, 127, 994

- Bailer-Jones C. A. L., Rybizki J., Founesneau M., Mantelet G., Andrae R., 2018, *AJ*, 156, 58
- Binney J. et al., 2014, *MNRAS*, 439, 1231
- Binney J., McMillan P., 2011, *MNRAS*, 413, 1889
- Binney J., Gerhard O., Spergel D., 1997, *MNRAS*, 288, 365
- Bond N. A. et al., 2010, *ApJ*, 716, 1
- Boubert D. et al., 2019, *MNRAS*, 486, 2618
- Brown A. G. A. et al., 2018, *A&A*, 616, A1
- Büdenbender A., van de Ven G., Watkins L. L., 2015, *MNRAS*, 452, 956
- Cui X.-Q. et al., 2012, *Res. Astron. Astrophys.*, 12, 1197
- Eddington A. S., 1915, *MNRAS*, 76, 37
- Evans N. W., Sanders J. L., Williams A. A., An J., Lynden-Bell D., Dehnen W., 2016, *MNRAS*, 456, 4506
- Foreman-Mackey D., Hogg D. W., Lang D., Goodman J., 2013, *PASP*, 125, 306
- Gómez F. A., Minchev I., O’Shea B. W., Beers T. C., Bullock J. S., Purcell C. W., 2013, *MNRAS*, 429, 159
- Gravity Collaboration et al., 2018, *A&A*, 615, L15
- Hagen J. H. J., Helmi A., de Zeeuw P. T., Posti L., 2019, preprint ([arXiv:1902.05268](https://arxiv.org/abs/1902.05268))(H19)
- Katz D. et al., 2019, *A&A*, 622, A205
- Khan S. et al., 2019, *A&A*, 628, A35
- Kunder A. et al., 2017, *AJ*, 153, 75
- Laporte C. F. P., Minchev I., Johnston K. V., Gómez F. A., 2019, *MNRAS*, 485, 3134
- Lindgren L. et al., 2018, *A&A*, 616, A2
- Luri X. et al., 2018, *A&A*, 616, A9
- Lutz T. E., Kelker D. H., 1973, *PASP*, 85, 573
- Queiroz A. B. A. et al., 2018, *MNRAS*, 476, 2556
- Riess A. G. et al., 2018, *ApJ*, 855, 136
- Saha K., Pfenniger D., Taam R. E., 2013, *ApJ*, 764, 123
- Schönrich R., 2012, *MNRAS*, 427, 274
- Schönrich R., Aumer M., 2017, *MNRAS*, 472, 3979
- Schönrich R., Binney J., Dehnen W., 2010, *MNRAS*, 403, 1829
- Schönrich R., McMillan P., Eyer L., 2019, *MNRAS*, 487, 3568(S19)
- Sellwood J. A., 2014, *Rev. Mod. Phys.*, 86, 1
- Silverwood H., Sivertsson S., Steger P., Read J. I., Bertone G., 2016, *MNRAS*, 459, 4191
- Sivertsson S., Silverwood H., Read J. I., Bertone G., Steger P., 2018, *MNRAS*, 478, 1677
- Smith M. C., Evans N. W., An J. H., 2009, *ApJ*, 698, 1110
- Steinmetz M. et al., 2006, *AJ*, 132, 1645
- Strömberg G., 1927, *ApJ*, 65, 238
- Wegg C., Gerhard O., Bieth M., 2019, *MNRAS*, 485, 3296
- Williams M. E. K. et al., 2013, *MNRAS*, 436, 101
- Xiang M.-S. et al., 2017, *MNRAS*, 467, 1890
- Xu Y., Newberg H. J., Carlin J. L., Liu C., Deng L., Li J., Schönrich R., Yanny B., 2015, *ApJ*, 801, 105
- Xu S., Zhang B., Reid M. J., Zheng X., Wang G., 2019, *ApJ*, 875, 114
- Yanny B. et al., 2009, *AJ*, 137, 4377
- Zinn J. C., Pinsonneault M. H., Huber D., Stello D., 2019, *ApJ*, 878, 136

This paper has been typeset from a $\text{\TeX}/\text{\LaTeX}$ file prepared by the author.